Journal of ELECTRONIC MATERIALS, Vol. 47, No. 1, 2018
DOI: 10.1007/s11664-017-5775-3
© 2017 The Minerals, Metals & Materials Society

On Ni/Au Alloyed Contacts to Mg-Doped GaN

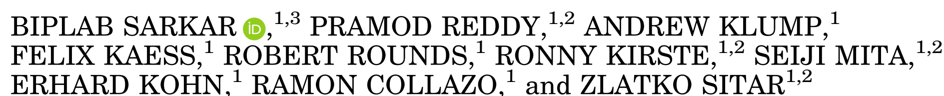
BIPLAB SARKAR,[1,3] PRAMOD REDDY,[1,2] ANDREW KLUMP,[1] FELIX KAESS,[1] ROBERT ROUNDS,[1] RONNY KIRSTE,[1,2] SEIJI MITA,[1,2] ERHARD KOHN,[1] RAMON COLLAZO,[1] and ZLATKO SITAR[1,2]

1.—Department of Materials Science and Engineering, North Carolina State University, Raleigh, NC 27695-7919, USA. 2.—Adroit Materials, 2054 Kildaire Farm Road, Suite 205, Cary, NC 27518, USA. 3.—e-mail: bsarkar@ncsu.edu

Ni/Au contacts to *p*-GaN were studied as a function of free hole concentration in GaN using planar transmission line measurement structures. All contacts showed a nonlinear behavior, which became stronger for lower doping concentrations. Electrical and structural analysis indicated that the current conduction between the contact and the *p*-GaN was through localized nano-sized clusters. Thus, the non-linear contact behavior can be well explained using the alloyed contact model. Two contributions to the contact resistance were identified: the spreading resistance in the semiconductor developed by the current crowding around the electrically active clusters, and diode-type behavior at the interface of the electrically active clusters with the semiconductor. Hence, the equivalent Ni/Au contact model consists of a diode and a resistor in series for each active cluster. The reduced barrier height observed in the measurements is thought to be generated by the extraction of Ga from the crystalline surface and localized formation of the Au:Ga phase. The alloyed contact analyses presented in this work are in good agreement with some of the commonly observed behavior of similar contacts described in the literature.

Key words: Alloyed contact, *p*-GaN, TLM, specific contact resistance

INTRODUCTION

Obtaining an ohmic contact to *p*-GaN is still a major challenge, primarily for two reasons: (1) a high acceptor activation energy in *p*-GaN resulting in very low free carrier concentration,[1] and (2) the presence of an electronic barrier between the metal contact and the *p*-GaN.[2] Typically, Ni/Au is used to form an ohmic contact on *p*-GaN by alloying in air at around 400–600°C, but many of the reported contact current–voltage (*I*–*V*) characteristics have been observed to be non-linear.[3] While some reports attribute the ohmic characteristics to the formation of a NiO-phase with semiconducting properties,[4,5] other reports claim that the formation of Au:Ga alloy phases at the *p*-GaN interface is responsible for the ohmic behavior.[6,7] Consequently, some reports claim current conduction to occur homogeneously through the entire contact area, whereas others propose conduction through isolated clusters.[3]

In addition to the disagreement on the conduction mechanism, the values of the specific contact resistance reported in the literature vary by several orders of magnitude.[8,9] Since the contact *I*–*V* characteristics, mostly obtained from planar transmission line measurement (TLM) structures, show a non-linear behavior, the contact resistance needs to be extracted following additional mathematical analysis.[10] On the other hand, transmission electron microscopy (TEM) studies showing a heterogeneous interface between the GaN and a grainy metal overlayer[11,12] have been used as supporting evidence for the formation of an alloyed contact configuration; however, a clear understanding of the current conduction mechanism across the *p*-GaN/metal interface has not yet emerged.

(Received May 15, 2017; accepted August 29, 2017; published online September 8, 2017)

This work studies contact formation to differently doped *p*-GaN by examining *I*–*V* curves, interface morphology, and interface chemistry of the annealed Ni/Au metal stacks. A non-linear contact analysis method was employed to identify the diode-type and resistor-type contribution of the contacts in TLM geometry. Finally, the non-linearity and contact resistance dependence on free carrier concentration was observed to emerge due to alloyed contact formation on *p*-GaN. The alloyed contact analyses are in good agreement with measurements and behavior commonly observed in the literature.

EXPERIMENTAL

Mg-doped *c*-plane oriented GaN layers with free hole concentrations between 1.1×10^{17} and 5.3×10^{18} cm^{-3} were grown on sapphire and single crystal AlN substrates using a metalorganic chemical vapor deposition (MOCVD) technique by a vertical, cold-walled, rf-heated reactor. Ammonia and triethylgallium (TEG) were used as precursor gases. For doping, bis-cyclopentadienyl magnesium (Cp_2Mg) was used as a magnesium precursor. Further details on MOCVD growth of *p*-GaN can be found elsewhere.[13–15] After growth, all samples were activated with a 700°C, 20-min anneal in air ambient. Following the activation, samples were cleaned using acetone, methanol, and deionized (DI) water, followed by dipping in 1% HF and hot 1:1 HCl:H_2O solution. Next, 100×200 μm^2 TLM contact pads were formed on the activated samples using conventional photolithography and Ni (20 nm)/Au (40 nm) metal deposition by e-beam evaporation in UHV (base pressure 1×10^{-9} Torr). The contacts were then annealed at 600°C for 10 min in air. Hall measurements (using Van der Pauw geometry) were performed to estimate the free hole concentration (p), mobility (μ) and resistivity (ρ) of different *p*-GaN samples.

To verify the formation of an interfacial alloying front, the Ni/Au contact metallization was removed from the samples using hot aqua regia (3:1 HCl:HNO_3), and the surface was analyzed by atomic force microscopy (AFM). Separately, x-ray photoelectron spectroscopy (XPS) was performed on a thin Ni/Au contact on *p*-GaN to examine the contact interface chemistry. *I*–*V* measurements were performed using a Keithley 4200 SCS. All data in this study were taken at room temperature.

RESULTS AND DISCUSSION

TLM analysis allows for the extraction of the contact resistance from a planar configuration. For Ni/Au contacts on *p*-GaN, the *I*–*V* characteristics appeared to be roughly linear when the distance between the contact pads was relatively large, as shown in Fig. 1a. However, the non-linearity became obvious as the pad distance is decreased. In a first-order approximation, the *I*–*V* characteristics shows a threshold characteristics at low voltages, followed by a nearly linear *I*–*V* relationship at higher voltages representing the resistance of the semiconductor channel underneath the contact. Thus, for the case of non-linear *I*–*V* characteristics, the conduction path consists of two back-to-back diodes, and the contact resistance should be extracted from the *I*–*V* characteristics segment after the reverse-biased diode breaks down (as shown in Fig. 1a). Consequently, in an equivalent circuit model, the planar resistance needs to be represented by a lateral resistive transmission line in the semiconductor, in conjunction with laterally distributed interfacial metal semiconductor junctions consisting of local contact resistance in series with a diode, as shown in Fig. 1b. The purpose of representing several diodes in series with resistors for each Ni/Au contact is to represent the alloyed contact model, which will be discussed later in this paper. Thus, equivalent contact seems to have a diode in series with a resistor for each Ni/Au contact (as shown in Fig. 1a); however, each diode represents several diodes connected in parallel configuration in the actual contact model (as shown in Fig. 1b). Note that the *I*–*V* characteristics are symmetrical, implying that, when one contact goes into reverse breakdown, the other contact is forward-biased. Therefore, the threshold component in the *I*–*V* characteristics is representative of the reverse breakdown of diodes (indicated by a reverse breakdown voltage, V_{RBD}, in Fig. 1a) after which the current is limited by the resistive contributions. Hence, the contacts are highly resistive until the reverse-biased diode goes into breakdown, and contact resistance measurements at voltages lower than V_{RBD} can be misleading. A least square fit of the current has been used to estimate the resistive contribution (R), whereas the x-intercept has been used to estimate the values of V_{RBD}.

This non-linear contact analysis using diode and resistive contributions was employed to determine the dependence of all circuit parameters (namely, the channel sheet resistance, contact resistance, and the non-linear junction properties) on free carrier concentration on different *p*-GaN samples. Figure 2a shows the *I*–*V* characteristics for Ni/Au contacts for samples with different free hole concentrations and a TLM pad distance of $\sim$15 μm. All elements, namely the channel sheet resistance, the contact resistance and the junction threshold voltage, showed dependence on free carrier concentration. It is important to note that the reverse and forward junctions are in series in the TLM pattern; the voltage drop across the forward-biased junction is usually neglected, as it is not directly accessible in a symmetric pattern.

As shown in Fig. 2b, the dependence of the V_{RBD} on free carrier concentration was roughly linear. This was expected as the reverse breakdown voltage should be related to the near surface depletion layer and, thus, scale with the free carrier concentration.[2]

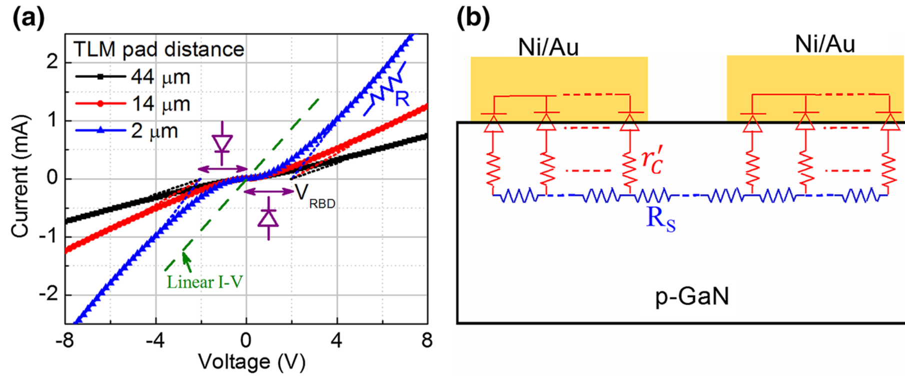

Fig. 1. (a) I–V characteristics of Ni/Au TLM structures on p-GaN with different contact spacing; (b) equivalent alloyed contact model of the Ni/Au TLM contact. Each diode represents a cluster site under the contact responsible for current conduction, and the contact resistance (R_c) extracted from the TLM analysis represents the parallel combination of resistances offered by the individual cluster site (r'_c).

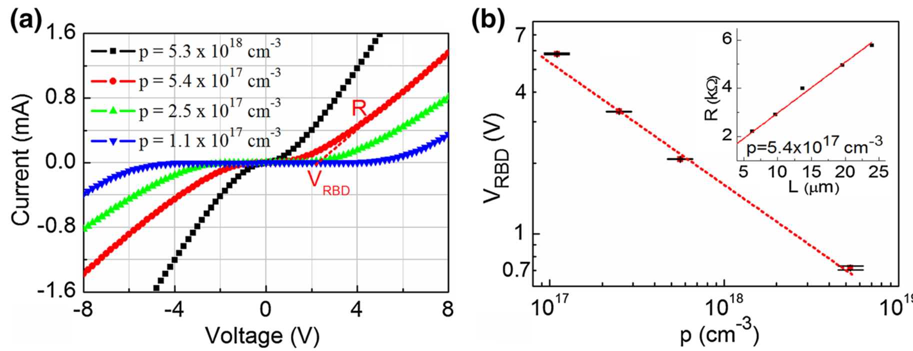

Fig. 2. (a) I–V characteristics of Ni/Au contacts on p-GaN with different free carrier concentrations (the dotted line shows the extraction of V_{RBD} and R for the sample with $p = 5.4 \times 10^{17}$ cm^{-3}); (b) dependence of the V_{RBD} on free carrier concentration, p. Inset shows the extraction of contact resistance for the sample with $p = 5.4 \times 10^{17}$ cm^{-3}.

As expected, V_{RBD} was independent of the channel length (contact spacing) and all I–V characteristics for a given carrier concentration showed similar V_{RBD}, regardless of the channel length (Fig. 1a). Also, the I–V characteristics were nearly linear after V_{RBD}, and the second order non-linear contribution was observed to be $<10\%$ of the linear contribution in the quadratic least square fit. The non-linearity may be arising due to factors like Joule heating at the current conduction site under the contact. Further, the error margin associated with the x-intercept (V_{RBD}) and the first-order coefficient of the least square fit (resistance, R) was observed to be $\leq 1\%$. The contact resistance, R_c, was extracted from the I–V characteristics above V_{RBD} with contact pad distance extrapolated to $L = 0$, as shown in the inset of Fig. 2b.

The specific contact resistance, ρ_c, was determined from Eq. 1, assuming that the sheet resistance underneath the contact was equal to the channel sheet resistance[16]:

$$\rho_c = \frac{R_c^2 w^2}{R_s} \tag{1}$$

where w is the width of the TLM pads (200 μm in this case) and R_s represents the sheet resistance of p-GaN (unit: $\Omega/\square$). Table I represent different contact analysis parameters obtained in this study.

Plotting the specific contact resistance (ρ_c) as a function of free carrier concentration resulted in an inverse linear relationship, as shown by the red squares in Fig. 3. Figure 3 also shows a comparison with the literature data for different types of contacts. Interestingly, literature reports on Ni/Au contacts on p-GaN show a similar tendency to the one determined here, albeit with significant scatter. Generally, higher free carrier concentration led to lower ρ_c. The inverse relationship between ρ_c and free carrier concentration is a fingerprint of classical alloyed contacts. In an alloyed contact, the interface between the distributed vertical junctions and the semiconductor channel is heterogeneous and can be modeled by a random distribution of active clusters responsible for the vertical current transfer. A model for such an alloyed contact configuration was first developed in the early 1980s by Braslau et al.,[38] who labeled active clusters as protrusions. A

Table I. Contact analysis parameters obtained from different *p*-GaN samples

p (cm^{-3})	μ (cm^2 V^{-1} s^{-1})	ρ (Ω cm)	ρ_c (Ω cm^2)
5.3×10^{18}	1.6	0.7	1.4×10^{-4}
5.4×10^{17}	9.6	1.2	1.8×10^{-3}
2.5×10^{17}	19.1	1.3	6.4×10^{-3}
1.1×10^{17}	21.4	2.6	1.6×10^{-2}

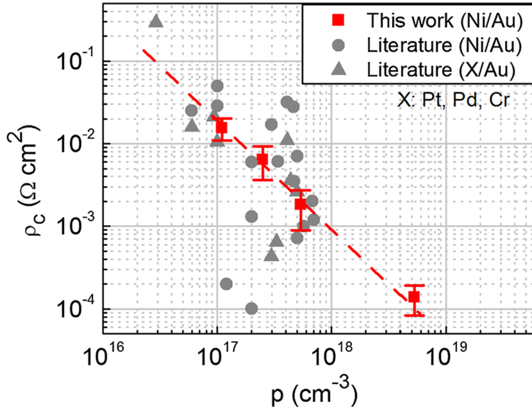

Fig. 3. Dependence of ρ_c on free carrier concentration, p, for different *p*-GaN samples. The plot also shows the literature reports of ρ_c for Ni/Au and X/Au contact, where X is Pt, Pd, or Cr.[5,8,9,16–37]

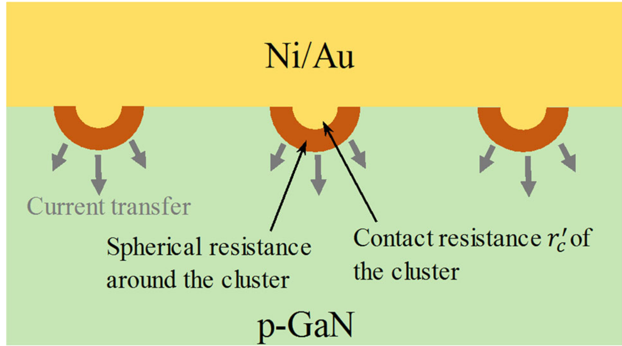

Fig. 4. Schematic of the alloyed contact model for Ni/Au contact on *p*-GaN. Active clusters surrounded by a spherical resistance act as the current transfer site.

schematic of the alloyed contact model for the Ni/Au contact on *p*-GaN is shown in Fig. 4.

Within this model, the specific contact resistance, ρ_c, has two components: (1) a series resistance in the semiconductor influenced by current crowding in the active clusters, and (2) a metal/semiconductor interface resistance around the electrically active protrusion. This is described as[38]:

$$\rho_c = a_p^2 \left[\frac{\rho}{\pi r_p} + \frac{r_c'}{2f\pi r_p^2} \right] \quad (2)$$

where a_p is the mean separation between the protrusions, r_p is the mean radius of the protrusions, r_c' is the specific contact resistance of protrusions, f is the field enhancement factor, and ρ is the resistivity of the semiconductor. The first term in Eq. 2 leads to an inverse relationship between the contact resistance and free carrier concentration. The second term can typically be neglected when considering a large field enhancement factor and an ideal tunneling through a thin barrier across the active protrusion interface.[38] However, in our case, the charge transfer from the metal to semiconductor does not seem to be by the ideal tunneling through a thin barrier, since a reverse breakdown threshold is observed in the *I–V* characteristics. Moreover, there is also a clear dependence of the reverse breakdown voltage on free carrier concentration as expected for the reverse breakdown of a metal/semiconductor junction (see Fig. 2). Thus, the active protrusions still bring about a residual interfacial barrier, and can be described as a combination of a diode and a resistor in series, as shown schematically in Fig. 1b. The model also indicates that a higher conductivity of *p*-GaN results in better contact formation.

All contacts compiled in Fig. 3 were annealed in air at moderate temperatures of around 600°C. According to the current understanding of contact formation in the Au/Ni/*p*-GaN system, annealing in air forms a stable nickel oxide phase (NiO),[4] with Au remaining intact. However, it has been observed that the metals undergo a reversal following the contact anneal, resulting in the formation of a Ni/Au/*p*-GaN interface.[4,11,17] It is speculated that the oxygen enters into the Ni film through the imperfections in the Au layer, creating local paths for the diffusion of Au towards the *p*-GaN surface.[4,12] Once Au reaches the *p*-GaN surface, it forms localized clusters of an Au:Ga alloy. As a result, Ga is leached out of GaN, generating a Ga-deficient interface,[3,7] which is thought to be responsible for a Ga-vacancy concentration profile that generates low-barrier, electrically-active clusters.

In order to gain some more insight into the contact formation mechanism, we removed the metallization following the contact anneal using a hot aqua regia solution, and as a control also subjected a pristine *p*-GaN film to the same chemical and anneal treatment. Figure 5 shows AFM topographs comparing the two etched *p*-GaN surfaces: (a) contact-free pristine surface and (b) contact formation and removal of the Ni/Au metallization. The contact-free surface showed a nearly defect-free step flow morphology with an associated RMS roughness of around 1 nm. After contact alloying, the step flow morphology was preserved with no increase in roughness, but the surface became decorated with nm-sized clusters (on the order of 100 nm). Note that the pristine *p*-GaN surface and the surface with the annealed Ni/Au contact were subjected to similar chemical treatments. The nearly defect-free surface observed in Fig. 5a clearly indicates that the pristine surface

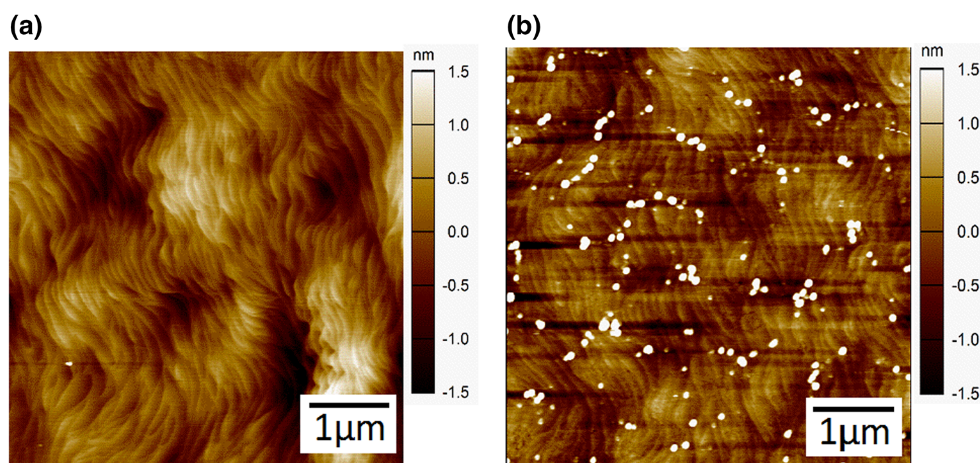

Fig. 5. AFM topography of (a) contact-free *p*-GaN surface, and (b) *p*-GaN surface after removing the Ni/Au contact.

was preserved even after exposing the sample to several anneal and chemical treatments, and that the formation of clusters solely due to a chemical reaction with the *p*-GaN surface could be excluded. Thus, the AFM topography in Fig. 5b has to be related to the contact formation which suggests that the contact formation is not uniform but rather in isolated clusters, which facilitate current flow. This would be consistent with the expectation that these nm-sized defects represent the alloying front of the electrically-active clusters that act as the current transfer sites. The shadows observed in Fig. 5b near the clusters were due to the height of the pillar-like clusters where the AFM tip deflects more than the surface step height. To a first-order approximation of Eq. 2 (considering $r_p \approx$ 30–50 nm), the value of mean separation (a_p) between the clusters becomes ~1–2 μm, which is in a good agreement with the cluster topography observed in Fig. 5b.

Further, to gain some insight into the interface chemistry between the *p*-GaN and metallization, a thin Ni (1.5 nm)/Au (3 nm) contact was deposited on *p*-GaN by e-beam evaporation in UHV and annealed in air at 600°C. The thinness and porosity of the contact allowed for the XPS investigation of the interface; details on determining the Schottky barriers and the chemical state of the surface elements are described elsewhere.[39] It was found that a lower Ga 3d binding energy generally indicates a lower Schottky barrier and that a chemical change of Ga from the nitride to metal results in a decrease of the Ga 3d binding energy.[40] A perusal of the XPS scan presented in Fig. 6 reveals the main Ga 3d peak from *p*-GaN at ~19.2 eV and the emergence of a shoulder on the low-energy side. Deconvolution and quantitative analysis of the two peaks reveal that the intensity ratio is similar to the surface cluster coverage in Fig. 5b. In addition, the binding energy of 17.4 eV reveals the possibly metallic nature of the shoulder peak corresponding to Au:Ga alloy. Further, this finding also qualitatively supports the cluster formation model where Ga is extracted from the *p*-GaN lattice during the alloying process, producing field enhancement depletion regions that reduce the effective Schottky barrier (~0.4 eV). Thus, the clusters observed in the AFM images seem to represent the areas where Au has leached Ga out the *p*-GaN lattice to form an Au:Ga alloy and a current transfer site. Note that the *I–V* characteristics observed in Fig. 2a are marginally asymmetric, and the asymmetry may be caused by factors like lithography-induced pad-to-pad variation and minor variation in the barrier height or cluster size under the contact.

Finally, the hypothesis of clustered contact formation on *p*-GaN was verified by current conduction through a non-annealed Ni/Au contact deposited on intentionally formed Au:Ga phases. For this, a 30-nm Au was deposited on an activated *p*-GaN sample, and was annealed at 650°C for 15 min under vacuum to avoid any oxidation. In this process, Ga is expected to diffuse into Au resulting in the formation of Au:Ga phases at the interface of *p*-GaN, as verified by the XPS studies. Au was then removed using boiling aqua regia solution. Ni/Au TLM contacts were then deposited and patterned, but the contacts were not annealed. For comparison, a standard Ni/Au contact was also deposited on a control sample taken from the same *p*-GaN wafer. The control sample was annealed at 600°C for 10 min at air ambient for contact formation (similar process steps were followed in Fig. 2). Figure 7 shows the comparison of current through the non-annealed Ni/Au contact and the standard Ni/Au contact having a similar TLM pad distance. The non-annealed Ni/Au contact showed comparable current conduction to that of the standard Ni/Au annealed contact. Thus, conduction through the non-annealed Ni/Au contact can be attributed to the formation of clustered Au:Ga phases formed after annealing Au on *p*-GaN, consistent with the AFM analysis shown in Fig. 5. Consequently, the Ni/Au contact showed conduction through these clusters without a contact anneal. A higher current and lower reverse breakdown voltage in the non-

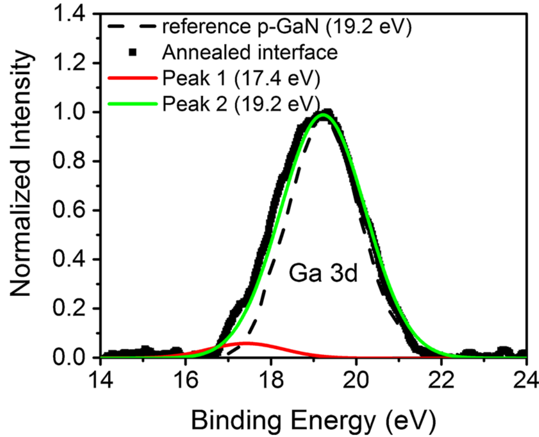

Fig. 6. Comparative XPS analysis of Ga 3d core level between reference *p*-GaN surface and annealed interface of thin Ni/Au contact on *p*-GaN showing the emergence of an additional low binding energy peak after the alloying process.

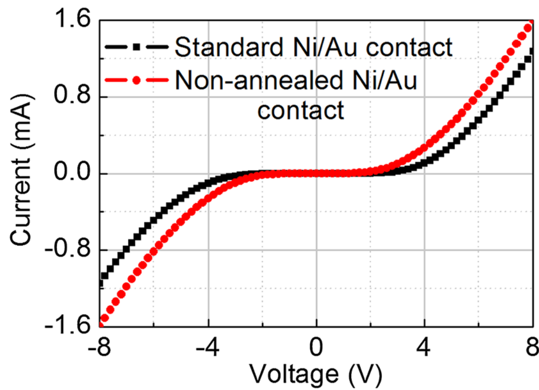

Fig. 7. Current through *p*-GaN with the standard Ni/Au contact and the Au-treated non-annealed Ni/Au contact.

annealed Ni/Au contact sample may be due to the formation of clusters with a higher field enhancement, or the generation of higher numbers of Au:Ga phases at the interface. Wang et al. recently reported a similar non-annealed contact formation on *p*-GaN after removing the previously annealed contact.[41] All these point toward optimization techniques that can be adopted to achieve a superior contact performance. Thus, the alloyed contact model analysis seems to be in a good agreement with some of the common observations in Ni/Au contact formation on *p*-GaN: the metal reversal during the contact anneal,[11] formation of isolated clusters,[4] dissolution of Ga into Au or formation of Au:Ga alloy phases,[7] etc. This conclusion implies the necessary timing requirements: (1) the oxidation should be limited to the Ni while the Ga-oxide formation should be avoided, and (2) it should allow for metal reversal and the formation of the Au:Ga alloy.

The following discussion can be added based on this structural information and the electrical performance analyses of Ni/Au contact to *p*-GaN. The nm-sized active clusters with a low barrier height (∼0.4 eV) surrounded by a high barrier height periphery (of approx. 2 eV) will indeed result in a strong spherical current distribution and a very small turn-on voltage in the forward direction. Thus, it seems justified to neglect a barrier behavior in the forward-biased part of the TLM contact pair. On the other hand, the cluster may be electrically pinched off at high reverse bias by the surrounding space charge layer, resulting in a relatively high reverse breakdown voltage depending on the free carrier concentration. To minimize any contact nonlinearity, two conflicting requirements need to be balanced: in reverse, pinch-off needs to be avoided, thus cluster size, doping level and associated free carrier concentrations need to be above a minimum critical value; while in the forward direction, a high current injection enhancement factor is necessary, making nm clusters preferable.

CONCLUSIONS

Non-linear behavior of the Ni/Au contacts to *p*-GaN annealed in air at 600°C was studied. TLM contact analysis showed a threshold characteristics at low voltages, followed by a nearly linear *I*–*V* relationship at higher voltages. Both electrical and structural analyses suggested classical alloyed contact formation with active clusters responsible for a localized current transfer. A contact spreading resistance generated by the current crowding at the active cluster could be identified, yielding a linear relationship of contact resistance with inverse free carrier concentration. Hence, the equivalent contact model consists of a diode in series with a resistor representing the diode-type and resistor-type contribution from each active cluster. The formation of Au:Ga alloy phases after the contact anneal is thought to result in a reduction of the local barrier height of the active clusters. The active current transfer sites show three distinct characteristics: (1) a high current injection efficiency under the forward bias resulting in current crowding and an associated semiconductor spreading resistance, proportional to the inverse of the free carrier concentration in the bulk, (2) a residual barrier of the transfer site with very small turn-on voltage in the forward bias condition, and (3) a free carrier-dependent reverse breakdown behavior. The alloyed contact analyses based on the above observations are also in a good qualitative agreement with commonly observed behavior described in the literature. While the presented model gives important qualitative insight into Ni/Au contact formation to *p*-GaN, much more work is needed for the development of a quantitative model.

ACKNOWLEDGEMENTS

We sincerely thank the support from NSF (ECCS-1610992, DMR-1312582, ECCS-1508854, DMR-

1508191) and ARO (W911NF-15-2-0068, W911NF-16-C-0101) for funding this work.

REFERENCES

1. Y. Chen, H. Wu, G. Yue, Z. Chen, Z. Zheng, Z. Wu, G. Wang, and H. Jiang, *Phys. Status Solidi B* 252, 1109 (2015).
2. J.-S. Jang and T.-Y. Seong, *Appl. Phys. Lett.* 76, 2743 (2000).
3. J. Chen and W.D. Brewer, *Adv. Electron. Mater.* 1, 1500113 (2015).
4. L.-C. Chen, F.-R. Chen, J.-J. Kai, L. Chang, J.-K. Ho, C.-S. Jong, C.C. Chiu, C.-N. Huang, C.-Y. Chen, and K.-K. Shih, *J. Appl. Phys.* 86, 3826 (1999).
5. J.-K. Ho, C.-S. Jong, C.C. Chiu, C.-N. Huang, C.-Y. Chen, and K.-K. Shih, *Appl. Phys. Lett.* 74, 1275 (1999).
6. H.W. Jang, S.Y. Kim, and J.-L. Lee, *J. Appl. Phys.* 94, 1748 (2003).
7. J.-L. Yang and J.S. Chen, *J. Alloys Compd.* 419, 312 (2006).
8. D. Qiao, L.S. Yu, S.S. Lau, J.Y. Lin, H.X. Jiang, and T.E. Haynes, *J. Appl. Phys.* 88, 4196 (2000).
9. Y. Tang, D. You, J. Xu, X. Li, X. Li, and H. Gong, *Semicond. Sci. Technol.* 21, 1597 (2006).
10. R. Wenzel, G.G. Fischer, and R. Schmid-Fetzer, *Mater. Sci. Semicond. Process.* 4, 357 (2001).
11. H. Omiya, F.A. Ponce, H. Marui, S. Tanaka, and T. Mukai, *Appl. Phys. Lett.* 85, 6143 (2004).
12. S.P. Lee, H.W. Jang, D.Y. Noh, and H.C. Kang, *Appl. Phys. Lett.* 91, 201905 (2007).
13. Z. Bryan, M. Hoffmann, J. Tweedie, R. Kirste, G. Callsen, I. Bryan, A. Rice, M. Bobea, S. Mita, J. Xie, Z. Sitar, and R. Collazo, *J. Electron. Mater.* 42, 815 (2013).
14. R. Kirste, M.P. Hoffmann, J. Tweedie, Z. Bryan, G. Callsen, T. Kure, C. Nenstiel, M.R. Wagner, R. Collazo, A. Hoffmann, and Z. Sitar, *J. Appl. Phys.* 113, 103504 (2013).
15. S. Mita, R. Collazo, A. Rice, R.F. Dalmau, and Z. Sitar, *J. Appl. Phys.* 104, 013521 (2008).
16. C.Y. Hu, Z.X. Qin, Z.X. Feng, Z.Z. Chen, Z.B. Ding, Z.J. Yang, T.J. Yu, X.D. Hu, S.D. Yao, and G.Y. Zhang, *Mater. Sci. Eng. B* 128, 37 (2006).
17. N. Braslau, *J. Vac. Sci. Technol.* 19, 803 (1981).
18. J.-K. Ho, C.-S. Jong, C.C. Chiu, C.-N. Huang, K.-K. Shih, L.-C. Chen, F.-R. Chen, and J.-J. Kai, *J. Appl. Phys.* 86, 4491 (1999).
19. D. Mistele, F. Fedler, H. Klausing, T. Rotter, J. Stemmer, O.K. Semchinova, and J. Aderhold, *J. Cryst. Growth* 230, 564 (2001).
20. M.-S. Oh, D.-K. Hwang, J.-H. Lim, C.-G. Kang, and S.-J. Park, *Appl. Phys. Lett.* 89, 042107 (2006).
21. G. Greco, P. Prystawko, M. Leszczyński, R.L. Nigro, V. Raineri, and F. Roccaforte, *J. Appl. Phys.* 110, 123703 (2011).
22. P.-S. Chen and C.-T. Lee, *J. Appl. Phys.* 100, 044510 (2006).
23. C.-S. Lee, Y.-J. Lin, and C.-T. Lee, *Appl. Phys. Lett.* 79, 3815 (2001).
24. Z.Z. Chen, Z.X. Qin, Y.Z. Tong, X.D. Hu, T.J. Yu, Z.J. Yang, X.M. Ding, Z.H. Li, and G.Y. Zhang, *Mater. Sci. Eng. B* 100, 199 (2003).
25. J. Liday, I. Hotový, H. Sitter, P. Vogrinčič, A. Vincze, I. Vávra, A. Šatka, G. Ecke, A. Bonanni, J. Breza, C. Simbrunner, and B. Plochberger, *J. Mater. Sci. Mater. Electron.* 19, 855 (2007).
26. D.J. King, L. Zhang, J.C. Ramer, S.D. Hersee, and L.F. Lester, MRS Proc. 468, 421 (1997).
27. F.G. Kalaitzakis, N.T. Pelekanos, P. Prystawko, M. Leszczynski, and G. Konstantinidis, *Appl. Phys. Lett.* 91, 261103 (2007).
28. H.W. Jang, T. Sands, and J.-L. Lee, *J. Appl. Phys.* 94, 3529 (2003).
29. J.K. Sheu, Y.K. Su, G.C. Chi, P.L. Koh, M.J. Jou, C.M. Chang, C.C. Liu, and W.C. Hung, *Appl. Phys. Lett.* 74, 2340 (1999).
30. P.-S. Chen, C.-S. Lee, J.-T. Yan, and C.-T. Lee, *Electrochem. Solid-State Lett.* 10, H165 (2007).
31. C.-F. Chu, C.C. Yu, Y.K. Wang, J.Y. Tsai, F.I. Lai, and S.C. Wang, *Appl. Phys. Lett.* 77, 3423 (2000).
32. S. Belahsene, G. Patriarche, D. Troadec, S. Sundaram, A. Ougazzaden, A. Martinez, and A. Ramdane, *J. Vac. Sci. Technol. B* 33, 010603 (2015).
33. J.-L. Lee, J.K. Kim, J.W. Lee, Y.J. Park, and T. Kim, *Solid-State Electron.* 43, 435 (1999).
34. J.K. Kim, J.-L. Lee, J.W. Lee, H.E. Shin, Y.J. Park, and T. Kim, *Appl. Phys. Lett.* 73, 2953 (1998).
35. D.-H. Youn, M. Hao, H. Sato, T. Sugahara, Y. Naoi, and S. Sakai, *Jpn. J. Appl. Phys.* 37, 1768 (1998).
36. H.W. Jang, K.H. Kim, J.K. Kim, S.-W. Hwang, J.J. Yang, K.J. Lee, S.-J. Son, and J.-L. Lee, *Appl. Phys. Lett.* 79, 1822 (2001).
37. J.-S. Jang, K.-H. Park, H.-K. Jang, H.-G. Kim, and S.-J. Park, *J. Vac. Sci. Technol. B* 16, 3105 (1998).
38. Y. Koide, T. Maeda, T. Kawakami, S. Fujita, T. Uemura, N. Shibata, and M. Murakami, *J. Electron. Mater.* 28, 341 (1999).
39. P. Reddy, I. Bryan, Z. Bryan, W. Guo, L. Hussey, R. Collazo, and Z. Sitar, *J. Appl. Phys.* 116, 123701 (2014).
40. D. Briggs and M.P. Seah, *Practical Surface Analysis by Auger and x-ray Photoelectron Spectroscopy* (New York: Wiley, 1983).
41. L. Wang, F. Wu, S. Liu, Q. Yang, Y. Zhao, D. Han, Z. Quan, and F. Jiang, *J. Appl. Phys.* 118, 165703 (2015).